Journal of Hydrology 603 (2021) 126839

Contents lists available at ScienceDirect

Journal of Hydrology

journal homepage: www.elsevier.com/locate/jhydrol

Research papers

PAHs sorption to biochar colloids changes their mobility over time

Wen Yang [a], Ting Qu [a], Markus Flury [b], Xin Zhang [a], Sigmund Gabriel [c], Jianying Shang [a,*], Baoguo Li [a]

[a] College of Land Science and Technology, China Agricultural University, Key Laboratory of Plant-Soil Interactions, Ministry of Education, and Key Laboratory of Arable Land Conservation (North China), Ministry of Agriculture, Beijing 100193, PR China
[b] Department of Crop and Soil Sciences, Washington State University, Pullman and Puyallup, Washington, USA
[c] Department of Environmental Geosciences and Environmental Science Research Network, University of Vienna, Althanstrasse 14, UZA2 1090 Vienna, Austria

ARTICLE INFO

This manuscript was handled by Huaming Guo Editor-in-Chief

Keywords:
Biochar Colloids
Transport
Kinetic Sorption
Naphthalene
Phenanthrene

ABSTRACT

Biochar is an efficient sorbent for polycyclic aromatic hydrocarbons (PAHs). However, little is known about PAHs sorption kinetics and the effect on the mobility of biochar colloids in saturated porous media. In this study, naphthalene (NAP) and phenanthrene (PHE) were chosen as typical PAHs. In different stages, different sorption sites of PAHs on biochar played a distinct role in affecting the transport of biochar colloids in saturated porous media. The biochar colloids showed less negative surface charge as the contact time between biochar colloids and PAHs increased from 0.017 h to 96 h, which led to the mobility of biochar colloids decreasing over time. But after 168 h contact time, the surface charge of biochar colloids became more negative again, and the inhibition effect of PAHs on biochar colloid transport was weakened. This was related to the sorption kinetics of PAHs on biochar colloids: (1) PAHs sorption onto outer biochar surface; and (2) adsorbed PAHs diffusion into internal biochar pores. PAHs sorption onto the outer biochar surface shielded the negative surface charge and then decreased the mobility of biochar colloids, and then the adsorbed PAHs diffusion into internal biochar pores increased their mobility again. Our results suggested that porous colloids-facilitated PAHs transport in porous media might be highly related to interaction time between PAHs and porous colloids.

1. Introduction

Polycyclic aromatic hydrocarbons (PAHs) are a ubiquitous group of organic contaminants, which consist of multiple aromatic rings and are produced by the incomplete combustion of carbon-containing materials. Naphthalene (NAP) and phenanthrene (PHE) are two typical PAHs (Soltani et al., 2015; Li et al., 2019). The content of PAHs in aquatic, soil, and sedimentary environments is increasing due to human activities. Because of their strong aromaticity and high hydrophobicity, PAHs mainly sorb onto geo-sorbents, i.e., soil, sediment, and black carbon (Cornelissen et al., 2006; An et al., 2017). The hydrophobicity of PAHs increases with the number of aromatic rings (Han et al., 2014; Yang et al., 2018; Zhu et al., 2018). Due to their high carcinogenicity, bio-accumulation, and poor degradation in the environment, PAHs have been listed as priority pollutants by the United States Environmental Protection Agency (USEPA) (Zhu et al., 2018; Ye et al., 2019).

Biochar was considered as an adsorbent for PAHs because of its high aromaticity, rich porous structure, and high specific surface area (Wang et al., 2006; Chen et al., 2008; Yargicoglu et al., 2015; Wang et al., 2017a). The immobilization of PAHs by biochar decreases their bioavailability (Beesley et al., 2010; Khan et al., 2015). Besides, biochar enhances PAHs degradation by increasing microbial activity (Anyika et al., 2015; Rein et al., 2016; Sigmund et al., 2018; Yang et al., 2018). Therefore, biochar can be used as a remediation agent in PAHs contaminated soil (Anyika et al., 2015). Biochar produced by high-temperature pyrolysis (>400 °C) has more condensed aromatic clusters and shows a strong affinity for PAHs through π-π electron-donor–acceptor interaction (Zhu and Pignatello, 2005; Wang et al., 2016; Wang et al., 2017a). High-temperature biochar generally has a large porosity with well-developed nano- or micro-pores , which are accessible for sorption of low molecular weight PAHs (LMW-PAHs) (Chen et al., 2012). Thus, pore-filling is one of the dominant mechanisms for LMW-PAHs sorption on biochar (Chen et al., 2008).

Biochar can be used as a passivant to remediate PAHs-contaminated soil. Biochar in the soil is always subject to aging (Mia et al., 2017). Physical aging is the most critical degradation pathway for biochar

* Corresponding author.
E-mail address: jyshang@cau.edu.cn (J. Shang).

https://doi.org/10.1016/j.jhydrol.2021.126839
Received 30 December 2020; Received in revised form 12 August 2021; Accepted 14 August 2021
Available online 19 August 2021

(Spokas et al., 2014), which leads to biochar breakdown (Byrne and Nagle, 1997; Gao and Wu, 2014) and become micro- and nano-sized fragments (Wang et al., 2013a), which was called as biochar colloids. These biochar colloids can vertically migrate through the soil profile with flowing water (Obia et al., 2017). In recent years, a few studies in the laboratory focused on the movement of biochar colloids in saturated sand columns (Zhang et al., 2010; Wang et al., 2013a; Wang et al., 2013b; Yang et al., 2017a; Yang et al., 2019a). Feedstock, pyrolysis temperature, and particle size of biochar, as well as ionic strength and pH conditions of background solution highly affect the transport of biochar colloids in saturated porous media (Zhang et al., 2010; Wang et al., 2013a; Wang et al., 2013b). Moreover, organic compounds have a distinct influence on the transport of biochar colloids in saturated porous media (Wang et al., 2013b; Yang et al., 2017a; Yang et al., 2019a).

Because of the strong affinity of biochar for organic pollutants (Chen et al., 2008; Liu et al., 2017), biochar colloids may serve as a carrier for the organic contaminants, facilitate their transport, and induce secondary pollution in the environment (Zhang et al., 2010). The presence of NAP could reduce the transport of biochar colloids because NAP was strongly sorbed to biochar and reduced the negative surface charge of the biochar colloids through charge shielding (Yang et al., 2017a; Yang et al., 2017b; Castan et al., 2019). Sulfamethazine, an antibiotic, could decrease the mobility of biochar colloids in quartz sand column under acidic and neutral pH conditions and increase their mobility under alkaline conditions since sulfamethazine sorption changed the surface properties of biochar colloids (Yang et al., 2020). Hameed et al. (2021) have demonstrated that the mobilities of three typical organic contaminants (PHE, atrazine, and oxytetracycline) were very low but significantly increased by their co-transport with biochar colloids in the soil column. This suggested that the sorption process of organic contaminants on biochar colloids played an important role in the mobility and fate of biochar colloids in PAHs-polluted soil.

The adsorption of PAHs on biochar is a dynamic process. Previous studies have shown that rapid sorption occurs at the beginning of the interaction between biochar and PAHs in solution conditions, and slow adsorption is followed, which is limited by diffusion of LMW-PAHs into the internal pores of biochar (Chen et al., 2012; Liu et al., 2017). For PAHs adsorption on biochar, the time to reach the equilibrium of PAHs to biochar can range from hours (4.7 h for NAP) to days (1–18 days for PHE) (Chen et al., 2012; Yakout et al., 2013; Kang et al., 2017). For most antibiotics like lincomycin (Liu et al., 2016), sulfamethoxazole (Lian et al., 2014), tetracycline (Wang et al., 2017b), and ciprofloxacin (Shang et al., 2016), sorption equilibration time with biochar also varied from hours to days. In some experiments, pore diffusion could not be estimated due to short period.

In this study, the effect of PAHs sorption kinetics on the transport of biochar colloids in saturated sand columns was investigated. Two typical PAHs (NAP and PHE) were selected in our study due to their common presence in the polluted soil and wastewater (Cao et al., 2019; Wu et al., 2019). The adsorption and desorption characteristics of PAHs on biochar were quantified using batch experiments. To estimate the surface property change of biochar colloids with PAHs sorption kinetics over time, the electrophoretic mobility and infra-red spectrum characteristics of biochar colloids were measured at different contact time between biochar and PAHs. Column experiments were carried out to assess the mobility of biochar colloids in the presence of PAHs during different kinetic sorption stages. The objectives of this study were to: (1) study the influence of PAHs sorption kinetics on the surface physicochemical properties of biochar colloids; (2) explore the mechanism of kinetic sorption affecting the transport of biochar colloids in the presence of PAHs over time under saturated flow conditions.

2. Materials and methods

2.1. Biochar colloids

Biochar was produced by filling wheat straw (Zhengzhou, Henan Province, China) into a stainless-steel tank in a muffle furnace chamber purged with nitrogen. The temperature was increased by 20 °C min^{-1} and maintained at 600 °C for 1 h (Yang et al., 2017a; Yang et al., 2019a). Biochar colloids were obtained by repeated ball milling until the particle size was less than 500 nm. The grounded biochar powder was suspended in ultrapure water at a concentration of 50 mg L^{-1} and then sonicated for 10 min before use. The hydrodynamic diameter distribution of biochar colloidal suspensions was determined through dynamic light scattering (DLS) method using a Zetasizer (Nano ZS90, Malvern, UK).

The particle size and morphology of the grounded biochar colloids were measured by scanning electron microscope (SEM, Nova NanoSEM430, FEI, USA). The surface area and pore size distribution of the biochar colloids were characterized by the Brunauer-Emmett-Teller (BET) and Barrett-Joyner-Halenda (BJH) methods (ASAP2020, Micromeritics Instrument, USA). The elemental content, ash content, static contact angles, and functional groups of this biochar were reported previously (Yang et al., 2017a; Yang et al., 2017b; Yang et al., 2019a; Yang et al., 2020). The elemental composition of biochar colloids was also analyzed by X-ray photoelectron spectroscopy (XPS, ESCALAB 250Xi, Thermo Fisher Scientific, USA), and the XPS spectra were deconvoluted using a Gaussian-Lorentzian curve-fitting program (XPSPEAK 4.1).

2.2. Naphthalene and phenanthrene

NAP (99%, 585711, J & K Scientific Ltd, Beijing, China) and PHE (98%, 24898161, Sigma Aldrich, US) stock solutions with the concentration of 1 g L^{-1} were prepared with 99.5% ethanol (Yang et al., 2017a; Yang et al., 2017b). PAHs stock solutions were placed in a 10-mL amber glass vial with a Teflon-lined screw cap at 4 °C in the dark and filled to the top to avoid the volatilization of PAHs and ethanol.

2.3. Adsorption and desorption experiments

The adsorption and desorption experiments were carried out in 20-mL amber glass vials with Teflon-lined caps. Sorption experiments were conducted using 500 mg L^{-1} biochar and NAP/PHE with different concentrations (1–12 mg L^{-1}) in 1 mM NaCl solution (pH 7) for 24 h shaking. For kinetic sorption experiments, the initial concentrations for NAP and PHE were fixed at 3 and 10 mg L^{-1}, respectively. The suspensions were shaken for different periods (from 0.017 h to 168 h). Every sample in the sorption experiments was repeated in triplicate. After adsorption, the suspensions were filtrated through 0.1 μm PTFE membranes (JVWP04700, MilliporeSigma, US) to separate biochar and non-sorbed PAHs in the suspension. The NAP filtrates were measured by UV–vis spectrophotometry (TU-1900, Persee, China) at a wavelength of 220 nm (Yang et al., 2019a), and the PHE concentrations were measured by fluorescence spectrophotometry (F97Pro, Lengguang Technology, China) at 275 nm excitation and 366 nm emission wavelengths. The calibration curves of NAP and PHE are provided in Fig. S1. The adsorption isotherms were analyzed with Langmuir and Freundlich models. The kinetic experiments were analyzed with pseudo-first-order, pseudo-second-order, and intraparticle diffusion kinetic models in Section S1 of the supporting information (SI).

In the desorption experiments (Section S2 in SI), the PAHs-sorbed biochars were added into 20 mL of 99.5% ethyl acetate and then ultrasonicated for 2.5 min (De Jesus et al., 2017). The obtained samples were filtered again, and the NAP/PHE concentration in the solution was diluted and measured as described as above. The samples in the desorption experiments were measured in duplicate.

Table 1
Selected characteristics of biochar colloids.

Properties	Method	Biochar
Chemical composition (wt %)	EA [a]	C (60.2), H (1.6), O (37.2), N (0.5), S (0.5) [b]
	XPS	C (63.9), O (20.7), N (1.4), S (1.0), Si (4.6)
Functional group	FTIR	–OH, C–H, C═O, C═C, Aromatic C–H [b]
Specific surface area (m^2 g^{-1})	BET	117
Total pore volume (cm^3 g^{-1})	BJH adsorption	0.04
Average pore diameter (nm)	BJH adsorption	5.9
Contact angle (°)	Water	123 ± 3 [c]
	Glycerol	100 ± 8 [c]
	n-decane	0 [c]

[a] Chemical composition of biochar was measured by elemental analysis.
[b] Data from Yang et al. (2017a).
[c] Data from Yang et al. (2020).

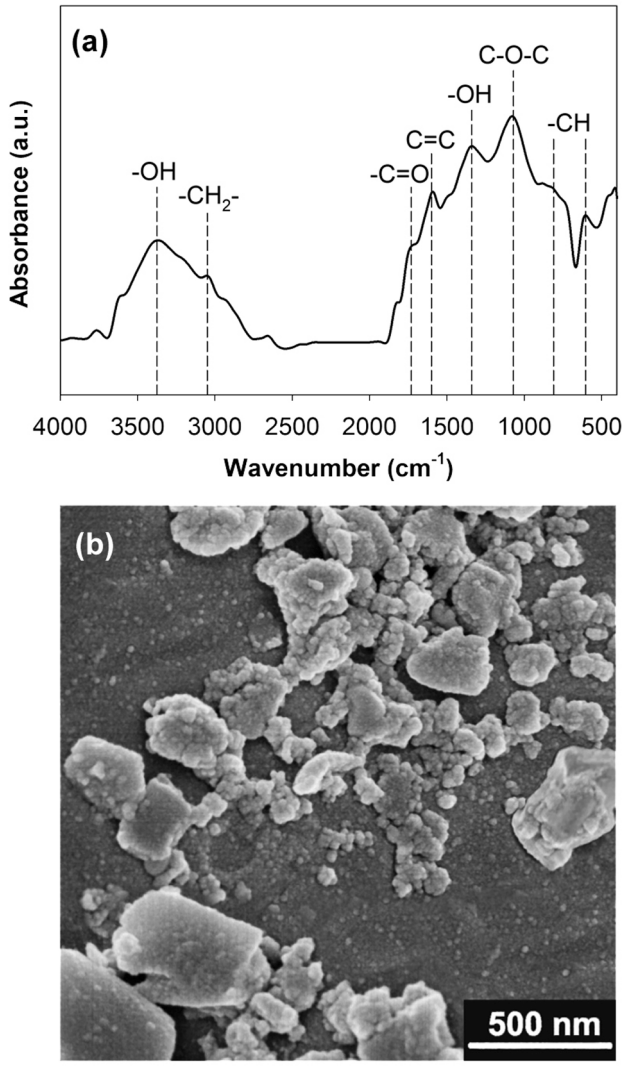

Fig. 1. (a) Fourier Transform Infrared (FTIR) spectra and (b) scanning electron microscope (SEM) image of biochar colloids.

2.4. Characterization of PAHs-sorbed biochar colloids

NAP or PHE stock solution (8 μL) was spiked into the 20 mg L^{-1} biochar colloidal suspension in 200-mL amber glass vials with a Teflon screw cap. The glass vials were orbitally shaken at 120 rpm for different contact time between biochar colloids and PAHs from 0.017 h (1 min) to 168 h. After shaking, the biochar suspensions were sonicated in a bath sonicator for 30 s. The zeta potentials (ζ) and hydrodynamic diameters of these biochar colloidal suspensions were measured with at least three independent measurements using a Zetasizer. The surface functional groups of biochar colloids were characterized by Attenuated Total internal Reflectance Fourier Transform Infrared (ATR-FTIR) spectroscopy (VERTEX 70, Bruker, Germany), and more details are given in Section S3 (SI).

2.5. Transport experiments

Transport experiments were carried out in a stainless-steel column with a diameter of 2.5 cm and a length of 12 cm, which was wet-packed with quartz sand (425 to 600 μm). The sand was cleaned by stirring in 2 M HCl for 24 h at 90 °C and thoroughly rinsed with ultrapure water before use (Sharma et al., 2008). The bulk densities of the packed columns ranged from 1.38 to 1.42 g cm^{-3}. To determine the ζ-potential of the quartz sand, the sand was ground into powder and then suspended in 1 mM NaCl solution. After 2-hour sedimentation, the suspended colloidal sand particles were used for ζ-potential measurements.

Transport experiments were conducted using a peristaltic pump to supply suspensions from bottom to top at a constant pore-water velocity of 0.44 cm min^{-1}. The column was initially equilibrated by injecting 5 pore volumes (PV) of 1 mM NaCl background solution, followed by 3 PVs of biochar colloid suspensions in the presence of PAHs. The biochar colloid suspensions (50 mg L^{-1}) with 0.1 mg L^{-1} NAP or PHE at different contact time (0.017, 24, 96, and 168 h) between biochar colloids were prepared in 1 mM NaCl solution. Then, several PVs of biochar-free background solutions were introduced into the column until no biochar could be detected in the effluent. The effluent was collected every 5 min using a fraction collector (BSZ-100, Huxi, China), and the biochar concentrations in the effluent were measured using a UV–vis spectrophotometer at a wavelength of 790 nm. All the column experiments were conducted in duplicate.

After transport experiments, the concentration of the biochar colloids in each column was determined by dividing the sand column into twelve increments, and the divided sands were then transferred into 50-mL conical flasks with 20 mL of ultrapure water and shaken at room temperature for 4 h to detach biochar colloids from the sand surface. The concentration of the biochar colloids in the suspensions was then measured by UV–vis spectrophotometry.

The one-dimensional colloid transport model using the convective–dispersive equation with two kinetic retention sites in the Hydrus-1D software (Šimunek et al., 1998; Bradford et al., 2003) was used to simulate the transport and retention of biochar colloids in the porous media (Section S4 in SI).

2.6. XDLVO theory

According to the extended Derjaguin-Landau-Verwey-Overbeek (XDLVO) theory, the interaction between biochar colloids and sand surface (Φ^{Total}) can be calculated as the sum of the van der Waals interaction (Φ^{LW}), the electrostatic double-layer interaction (Φ^{EDL}), and the acid-base interactions (Φ^{AB}). The detailed interaction calculations can be found in our previous study (Yang et al., 2017b).

Because the surface area of biochar which was shielded by NAP or PHE was very small compared with the whole surface, the effect of PAHs on the Hamaker constant and hydrophobicity of biochar colloids was negligible. In the presence of PAHs, the change of Φ^{Total} mainly came

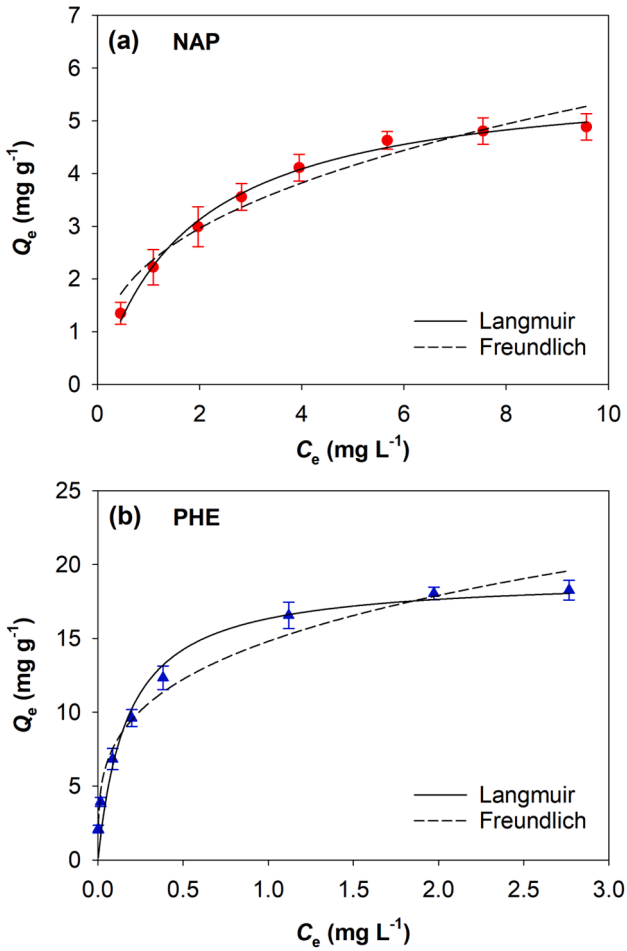

Fig. 2. Adsorption isotherms of (a) naphthalene (NAP) and (b) phenanthrene (PHE) on biochar after 24 h. Symbols represent mean values with standard deviations (n = 3). Lines are the model fittings.

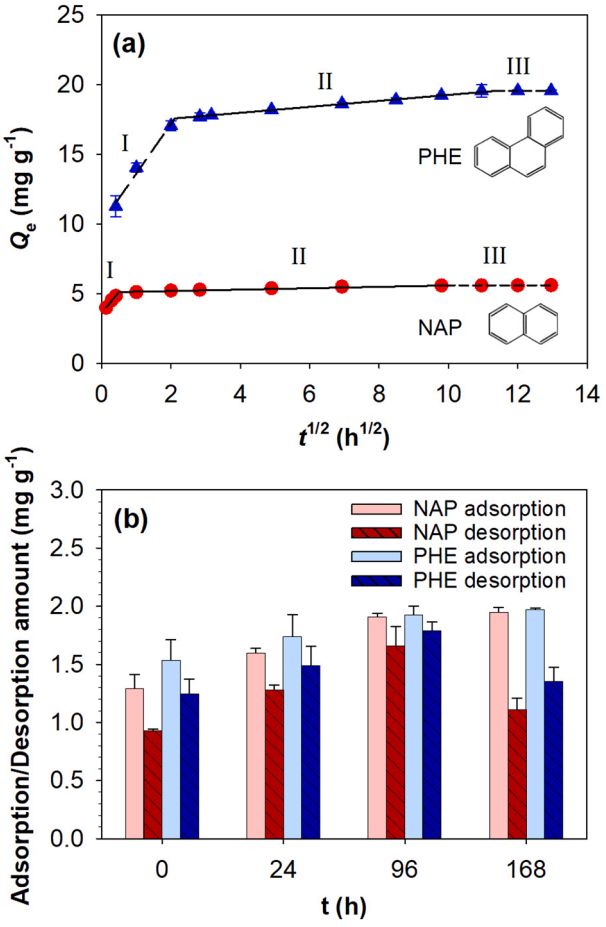

Fig. 3. (a) Intra-particle diffusion kinetics plots of naphthalene (NAP) and phenanthrene (PHE) to biochar; (b) adsorption and desorption of NAP and PHE on biochar in 1 mM NaCl solution as a function of contact time (0.017, 24, 96, and 168 h). Adsorption and desorption are depicted by the entire column in the graph, and error bars denote ± standard deviation (n = 2). Desorption samples were measured after 2.5 min ultrasonication in ethyl acetate.

from the Φ^{EDL} which was calculated by the zeta potentials of biochar colloids and sand in different experimental conditions.

2.7. Experimental attachment efficiency of biochar colloids to quartz sand

To quantitatively interpret the effect of PAHs sorption kinetics on the transport of biochar colloids, the experimental attachment efficiency (α) was calculated by the ratio of the rate of colloid deposition on a collector to the rate of collisions with that collector (Lecoanet and Wiesner, 2004):

$$\alpha = -\frac{2}{3}\frac{d_c}{(1-\varepsilon)L\eta_0}ln\left(\frac{C}{C_0}\right) \quad (1)$$

where d_c is the diameter of the quartz sand; ε is the porosity of the packed sand; L is the length of the column; C/C_0 is the ratio of colloids concentration in the effluent to that in the influent and can be obtained from the plateau of breakthrough curves; η_0 is the single-collector efficiency. Detailed calculation information can be found in Section S5 (SI).

3. Results and discussion

3.1. Properties of biochar and biochar colloids

The physicochemical characteristics of the biochar are summarized in Table 1. The C1s XPS spectrum (Fig. S2) was deconvoluted into four peaks, including C–C, C–H, aromatic C (~284.8 eV), C-O of phenolic hydroxyl or ether group (~286.2 eV), C═O of ketone group (~287.3 eV), and –COO of the carboxylic group (~289.0 eV) (Jin et al., 2017; Liu et al., 2017; Luo et al., 2017), which was in good agreement with the analysis of the FTIR spectra (Table 1, Fig. 1a). Biochar contained alkyl groups and aromatic C contributing to the hydrophobicity of biochar surface (Kinney et al., 2012; Liao et al., 2012). For high-temperature biochar (500–700 °C), high aromaticity may be linked to strong PAHs sorption affinity because of large electron-accepting capacity (Xiao et al., 2014). The presence of the O-containing functional groups resulted in a negative surface charge of the biochar in suspensions under pH > 4 conditions (Yang et al., 2019b). So, the isoelectric points (IEP) of biochars in solution were often less than 4 (Liu et al., 2016; Batista et al., 2018; Song et al., 2019).

According to SEM analysis, the biochar colloids showed an irregular granular shape (Fig. 1b), and the hydrodynamic particle size distribution of the colloids ranged from 255 to 615 nm, and the mean size was 422 ± 82 nm (Fig. S3). The pore volume of the biochar colloids was 0.04 cm^3 g^{-1}, and the average pore diameter was 5.9 nm (Table 1). The pore volumes of wheat straw biochar (600 °C) in literature ranged from 0.0092 to 0.11 cm^3 g^{-1} (Tang et al., 2015; Břendová et al., 2017; Leng et al., 2021). The difference in the pore volumes of biochar might be caused by different pyrolysis procedures of biochar production. The pore size distribution analysis showed a peak at a diameter of about 1.7–1.9

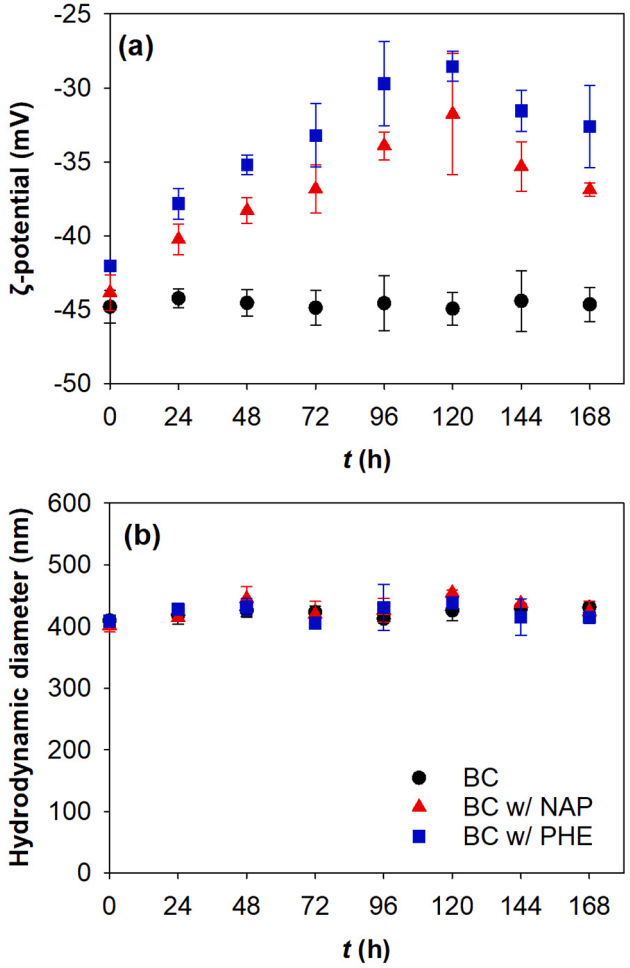

Fig. 4. (a) ζ-potentials and (b) hydrodynamic diameters of biochar colloids (BC) in the absence/presence of NAP/PHE in 1 mM NaCl solution as a function of contact time from 0.017 h to 168 h. Symbols represent mean values, and error bars denote ± standard deviation. NAP denotes naphthalene and PHE denotes phenanthrene.

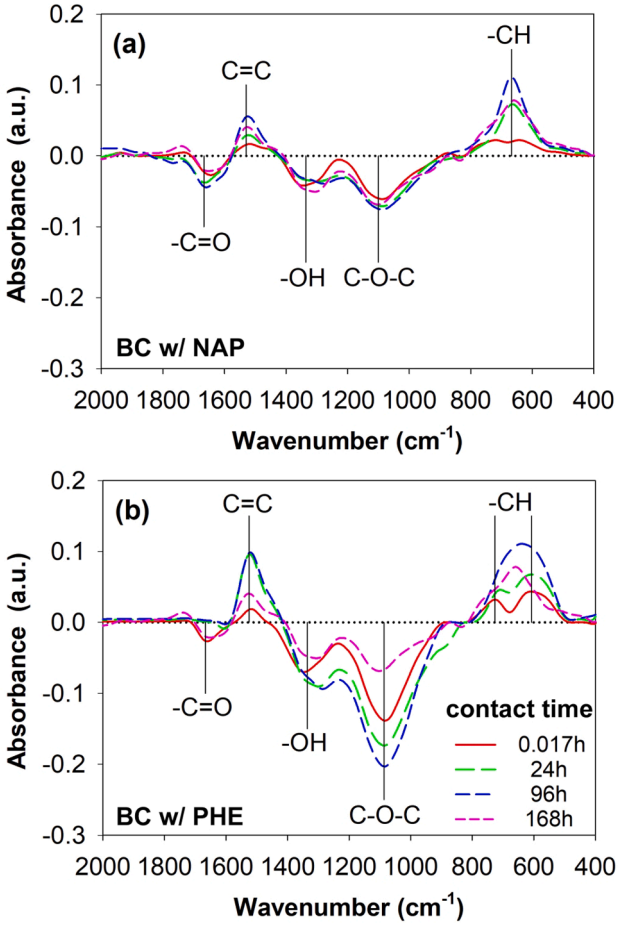

Fig. 5. Attenuated total reflection Fourier transform infrared (ATR-FTIR) spectra of NAP-sorbed (a) and PHE-sorbed (b) biochar colloids (BC) at different contact time (0.017, 24, 96, and 168 h). The biochar colloidal film in the absence of NAP/PHE was used as the reference for the ATR-FTIR spectra. NAP denotes naphthalene and PHE denotes phenanthrene.

nm and a tail after 10 nm (Fig. S4). This pore size distribution indicated that there were a large number of micropores and mesopores on the biochar, in which the micropores were dominant.

3.2. Kinetic adsorption and desorption of PAHs on biochar

The adsorption isotherms of NAP and PHE on biochar were well fitted by the Langmuir and Freundlich models (Fig. 2, Table S2). The adsorption isotherms were nonlinear, indicating that there were heterogeneous and limited sorption sites on biochar surfaces. The value of $1/n$ in the Freundlich isotherm was between 0.1 and 0.5, demonstrating that the adsorption of PAHs on biochar was favorable (Liu et al., 2016). According to the Langmuir model, the maximum adsorption capacities of biochar for NAP and PHE were 5.89 and 19.18 mg g^{-1}, respectively, which meant that the biochar showed a stronger sorption affinity for PHE. Oleszczuk et al. (2012) and Chan et al. (2020) also found that PHE adsorption by biochar in drinking water and sewage sludge was higher than that of NAP. The reason might be that more PHE could be sorbed onto biochar due to strong π-donor interaction than NAP (Zhu and Pignatello, 2005). The stronger adsorption affinity for PHE than for NAP had also been found in other materials, such as activated carbons (Bu et al., 2011; Yakout et al., 2013; Xiao et al., 2015; Eeshwarasinghe et al., 2018), graphene and graphene oxide nanosheets (Wang et al., 2014), and organoclay (Yin et al., 2019).

Sorption kinetics of both NAP and PHE onto biochar showed rapid initial sorption followed by slow sorption (Fig. S5). Compared with the pseudo-first-order model, the pseudo-second-order model shows a better regression fitting (Table S3), and similar findings have been reported in the previous studies (Tang et al., 2015; Zhang et al., 2015; Liu et al., 2017; Qiao et al., 2018). The theoretical Q_e values obtained from the pseudo-second-order model are similar to the Q_m values based on Langmuir models (Table S2). According to the simulation results using the intraparticle diffusion model (Eq. S5, SI), PAHs adsorption on biochar could be divided into three stages, and the sorption data were well fitted in each stage (Fig. 3a and Table S3). The first stage (0–0.17 h for NAP and 0–4 h for PHE) represented the rapid sorption of PAHs onto the external surfaces of biochar. The second stage (0.17–100 h for NAP and 4–120 h for PHE) was characterized by both PAHs adsorption onto external biochar surfaces and externally-sorbed PAHs diffusion into biochar micropores (Wang et al., 2017a; Zhu et al., 2018). In the third stage (100–168 h for NAP and 120–168 h for PHE), the sorption was dominated by PAHs intraparticle diffusion, and the sorption finally obtained equilibrium at 168 h. The sorption of other organic chemicals, such as methylene blue, tetracycline, doxycycline, and ciprofloxacin (Wang et al., 2018; Que et al., 2018; Zeng et al., 2018) onto biochar also showed similar three-stage sorption kinetic characteristics. The mechanisms of controlling PAHs sorption on biochar could be attributed to π-π electron-donor–acceptor interaction and pore-filling (Cornelissen and Gustafsson, 2005; Wang et al., 2016; Guo et al., 2017; Wang et al., 2017a).

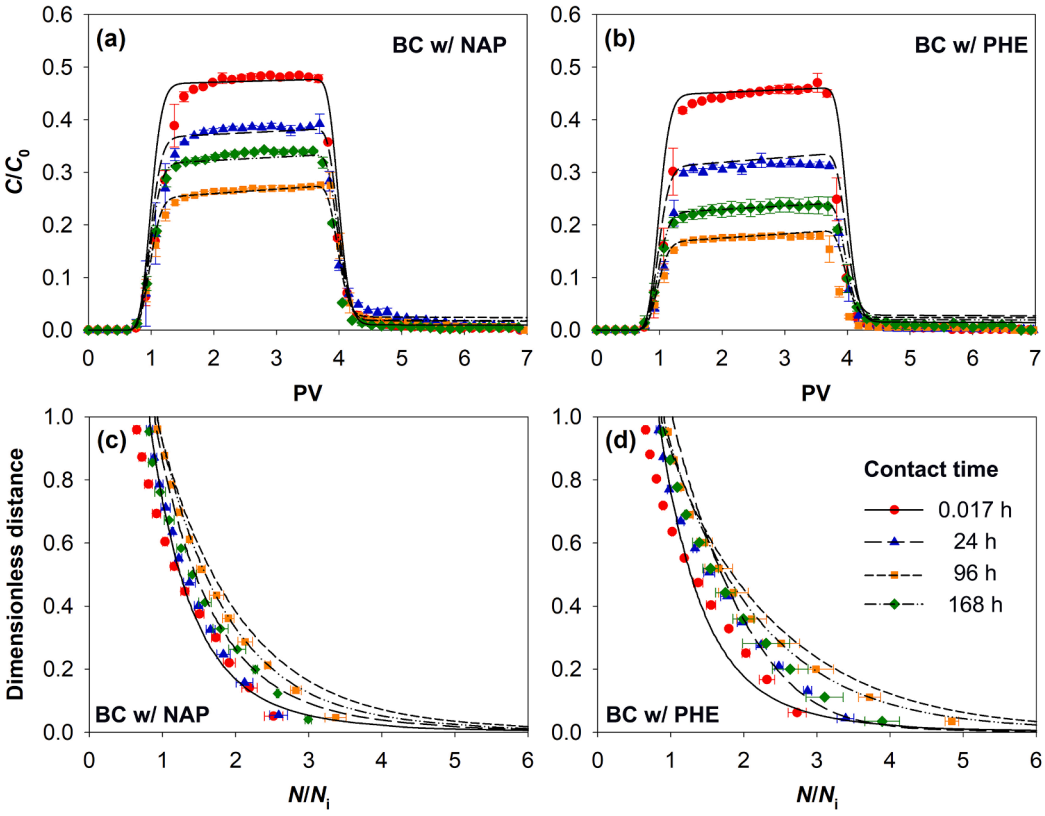

Fig. 6. Measured (symbols) and fitted (lines) breakthrough curves (top) and retention profiles (bottom) of biochar colloids (BC) in the presence of (a, b) NAP and (c, d) PHE in 1 mM NaCl solutions with different contact time (0.017, 24, 96, and 168 h). Symbols represent mean values, and error bars denote ± standard deviation (n = 2). NAP denotes naphthalene and PHE denotes phenanthrene. *C*: biochar colloids concentration in the effluents; C_0: injected biochar concentration; PV: the pore volume of the packed column; Dimensionless distance: the distance from column inlet; *N*: residual biochar colloids mass in one pore volume; N_i: biochar colloids mass in one pore volume of the injected biochar suspension.

The desorption of PAHs from biochar varied as a function of sorption time (Fig. 3b). After 96 h of adsorption, most of the NAP and PHE (about 87% and 93% respectively) could be desorbed because most of the PAHs were sorbed onto the external surface of biochar particles, and only a small amount of PAHs was retained in the internal pores of biochar particles. However, at 168 h contact time, only 57% of NAP and 69% of PHE could be desorbed, suggesting that the PAHs could not be easily desorbed from biochar after PAHs diffused into biochar internal pores. PAHs slow desorption from the biochar and other carbonaceous materials were highly related to intraparticle sorption (Yang et al., 2008; Kang et al., 2019). Sigmund et al. (2017) found that PAHs could diffuse into the small pores of the biochar leading to less accessibility for PAHs degradation. Liu et al. (2019) also showed that the desorbed lincomycin from biochar (pyrolyzed from rice hull bedding at 600 °C) was decreased from 62.4% to 8.8% as sorption time increased from 1 to 30 d.

3.3. *Effect of kinetic sorption on surface properties of biochar colloids*

The ζ-potential and hydrodynamic diameter of the biochar colloids in the absence of PAHs were around − 44.6 ± 1.2 mV and 422 ± 12 nm, and remained constant within 168 h (Fig. 4). After the immediate sorption (0.017 h) of NAP/PHE onto biochar colloids (i.e., PAHs were mixed and shaken with biochar colloidal suspension for 0.017 h), the ζ-potentials of the biochar colloids in the presence of PAHs were − 43.8 ± 1.2 mV for NAP and − 42.0 ± 0.3 mV for PHE, respectively. This was because after PAHs were added into biochar colloid suspension, a small amount of PAHs adsorbed on the external surface of the colloids immediately and shielded the parts of the negative surface charge (Yang et al., 2017a; Yang et al., 2017b). Compared with NAP, the charge shielding effect was more pronounced for PHE because PHE was strongly adsorbed by biochar (Fig. 2). With the increase of contact time between biochar colloids and PAHs from 0.017 h to 120 h, more PAHs were sorbed onto biochar colloids and the ζ-potential of biochar colloids in the presence of PAHs decreased to − 31.8 ± 4.1 mV for NAP and − 28.5 ± 1.0 mV for PHE. As the contact time increased from 120 h to 168 h, the ζ-potential of biochar colloids in the presence of PAHs decreased over time (−36.9 ± 0.4 mV for NAP and − 32.6 ± 2.8 mV for PHE at 168 h). The reason might be that less un-sorbed PAHs in the solution can be sorbed onto biochar surface at 168 h, and the PAHs, which were sorbed to the external surface of biochar, diffused into the intraparticle pores of biochar (Wang et al., 2017a; Zhu et al., 2018). This caused some negatively charged external surfaces of the biochar colloids to re-appear, which were previously shielded by PAHs. The hydrodynamic diameter of biochar colloids was not affected by sorption, which meant that PAHs sorption had no effect on the aggregation of biochar colloids in this case. Our results showed that after PAHs were added into biochar colloidal suspension, the hydrodynamic diameter of biochar colloids was almost constant and the negative surface charge changed with the PAHs sorption on biochar over time due to charge-shielding effect and intrapore diffusion.

The ATR-FTIR spectra of the biochar colloids in the presence of PAHs at different contact time periods also showed that the surface functional groups of biochar colloids changed with sorption kinetics (Fig. 5). After PAHs were sorbed to the colloids, the peaks around 1530 cm^{-1} (C═C stretching of aromatic skeletal C) and 800–600 cm^{-1} (aromatic C–H wagging vibrations) increased (Jia et al., 2018; Zhang et al., 2018) and the carboxylic peaks (including1667 cm^{-1} of aliphatic –C═O and 1336 cm^{-1} of carboxylic–OH) decreased (Chen et al., 2008; Gray et al., 2014),

Table 2
ζ-Potentials, hydrodynamic diameters of biochar colloids, and XDLVO energies between sand and biochar colloids with different PAHs equilibration time in 1 mM NaCl solutions.

C_{NAP}[a] (mg L^{-1})	C_{PHE}[b] (mg L^{-1})	t[c] (h)	d_{BC}[d] (nm)	ζ_{BC}[e] (mV)	Φ_{max}[f] (kT)	$\Phi_{min\ 2}$[g] (kT)
0	0	0.017	410 ± 2	−44.80 ± 1.10	356	−0.318
0	0	168	431 ± 10	−44.64 ± 1.15	354	−0.318
0.1	0	0.017	402 ± 10	−43.83 ± 1.20	346	−0.320
0.1	0	24	445 ± 19	−40.24 ± 1.05	312	−0.327
0.1	0	96	426 ± 20	−33.91 ± 0.94	249	−0.342
0.1	0	168	424 ± 18	−36.89 ± 0.45	279	−0.334
0	0.1	0.017	409 ± 2	−42.04 ± 0.28	329	−0.323
0	0.1	24	431 ± 14	−37.82 ± 1.04	288	−0.332
0	0.1	96	431 ± 37	−29.71 ± 2.86	207	−0.354
0	0.1	168	415 ± 5	−32.61 ± 2.76	236	−0.345

[a,b]Concentration of NAP/PHE in biochar colloid suspensions. NAP denotes naphthalene, and PHE denotes phenanthrene.
[c]Contacting time between biochar colloids and NAP/PHE.
[d]Hydrodynamic diameter of biochar colloids.
[e]ζ-Potentials of biochar colloids.
f,g Maximum primary energy barrier and secondary energy minimum for colloid-sand interaction, respectively. kT is a scaling factor for energy values in molecular-scale systems (Peter Atkins and De Paula, 2014).

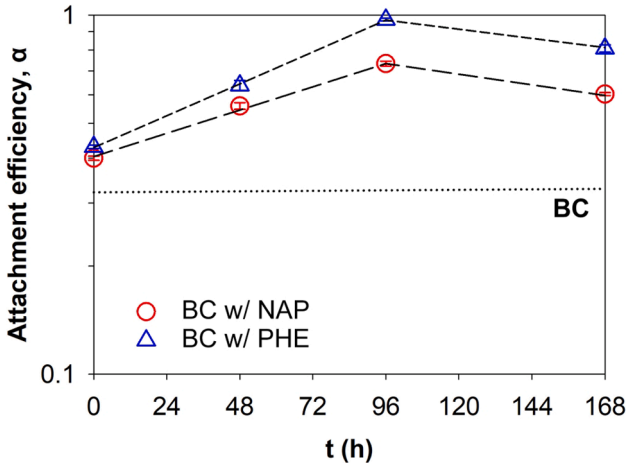

Fig. 7. The attachment efficiencies (α) of biochar colloids (BC) in the absence/presence of PAHs in 1 mM NaCl solutions as a function of contact time. NAP denotes naphthalene and PHE denotes phenanthrene.

indicating PAHs were sorbed onto the surface of biochar and shielded parts of the O-containing functional groups. The effect of PAHs sorption on the biochar functional groups increased with increasing contact time from 0.017 h to 96 h. As the contact time increased from 96 h to 168 h, the absorbance of all the functional groups on PAHs-sorbed biochar decreased due to the intraparticle diffusion of PAHs on the biochar.

3.4. Effect of kinetic adsorption on biochar colloid transport

The breakthrough curves and retention profiles of the biochar colloids in the presence of PAHs at different contact time periods are shown in Fig. 6, and the parameters of each column are listed in Table S4. The breakthrough curves showed the normalized biochar colloid concentration (C/C_0) in the effluent as a function of the pore volume. The experimental attachment efficiencies (α) were calculated from the breakthrough curves of biochar colloids using Eq. (1). The retention profile showed the ratio (N/N_i) of retained biochar colloids quality on the sand surface (N) to the quality of biochar colloids injected to the column (N_i) as a function of dimensionless distance from the column inlet.

Once 0.1 mg L^{-1} NAP or PHE was mixed with the biochar suspension for 0.017 h, the C/C_0 at the plateau of the breakthrough curves of biochar colloids decreased from 0.57 to 0.48 or 0.46, and the retained percentage of colloids in the column increased from 39% to 45% or 48% respectively (Figs. S6, 6, and Table S4). Our previous studies also showed that the mobility of biochar colloids was inhibited with increasing NAP concentration (Yang et al., 2017a; Yang et al., 2017b). This was because the sorbed NAP or PHE shielded the negative surface charge on the biochar colloids (Table 2), leading to a reduced electrostatic double-layer repulsion between biochar colloids and sand surface.

At different contact time between PAHs and biochar colloids, the breakthrough curves of biochar colloids showed different plateaus (Fig. 6a and b). The shaking time of bare biochar colloidal suspensions had no effect on biochar colloid transport in saturated sand column (Fig. S6). With the contact time between biochar colloids and PAHs increasing from 0.017 h to 24 h, and then to 96 h, the decrease of M_{eff} and the increase of the M_{ret} shown in Table S4 indicated that less biochar colloids were found in the effluents, and more colloids were retained in porous media. As more NAP or PHE adsorbed over time, the biochar colloids showed less negative surface charge (Fig. 4a). The less negative ζ-potentials resulted in a smaller primary energy barrier and a deeper secondary energy minimum between biochar colloids and quartz sand (Fig. S7, Table 2), which led to more colloid attachment on sand surfaces. However, when the contact time reached 168 h, the mobility of biochar colloids increased again, and fewer colloids were retained on the surface of the porous media (Fig. 6 and Table S4).

To exhibit the effect of PAHs sorption kinetics on the mobility of biochar colloids in porous media directly, the α values of biochar colloids at different contact time periods were calculated based on the C/C_0 of the breakthrough curves (Fig. 7). As the contact time increased from 0.017 h to 96 h, the α values of biochar colloids were increased about 25% for NAP, and 34% for PHE. When the contact time increased to 168 h, the α values of biochar colloids in the presence of PAHs decreased.

The breakthrough curves and retention profiles of biochar colloids in the presence of PAHs could be well simulated by the two-site kinetic retention model (Table S5). The values of the first-order attachment coefficient (k_1) on reversible kinetic retention site (site 1) became larger as PAHs sorbed onto biochar colloids and increased with increasing contact time from 0.017 h to 96 h, but decreased during 96–168 h. This indicated that the increase in PAHs sorbing onto the external surface of biochar resulted in an increase of colloid retention. The values of the first-order detachment coefficient (k_{1d}) on site 1 were one order of magnitude smaller than the attachment coefficient k_1. The values of the first-order attachment coefficients (k_2) on the irreversible kinetic retention site (site 2) were similar in every column experiment, implying that the retention of colloids on site 2 was mainly caused by colloid straining rather than attachment. Therefore, the impact of PAHs on the deposition of biochar colloid on quartz sand mainly occurred on the reversible kinetic retention site.

Nonpolar NAP and PHE can be effectively sorbed onto biochar surface through π-π electron-donor–acceptor interactions. The PAHs can sorb on both the external and internal surfaces of the biochar, and the external sorption is fast, followed by a rate-limited intraparticle diffusion (Li et al., 2014; Wang et al., 2017a; Zhu et al., 2018). As intraparticle diffusion plays the dominant role, the externally-sorbed PAHs on the outer biochar surface decreased with contact time (Fig. 8). At this stage, the sorption of PAHs on biochar changed the surface charge non-monotonically, and the mobility of biochar colloids was consequently

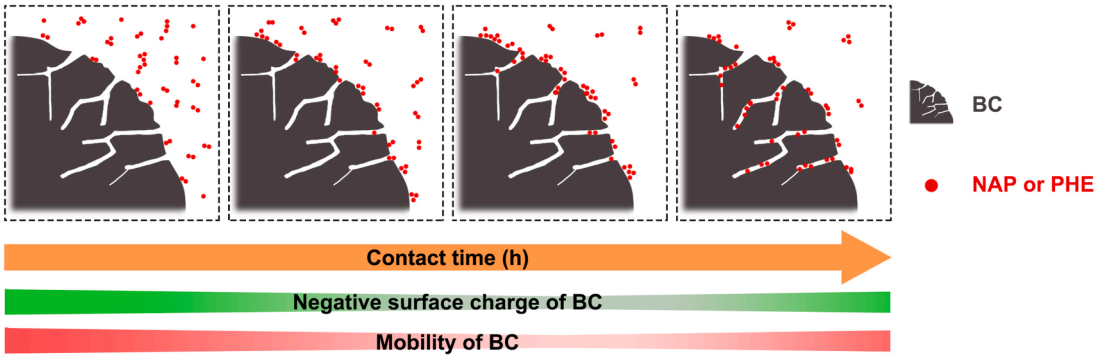

Fig. 8. Schematic of PAHs adsorption kinetics on biochar colloids (BC) and its related effects on surface charge and mobility.

affected.

To prove the effect of PAHs kinetic sorption on the mobility of biochar colloids, similar transport experiments were conducted in another rough sand (Figs. S8, S9), which confirmed that the mobility of biochar colloids was affected by PAHs kinetic sorption. The XDLVO energies between sand and biochar colloids and the fitted parameters of breakthrough curves are listed in Tables S6–S8. The breakthrough curves in Fig. S9 show more pronounced attachment and straining because the rough surface of the quartz sand provided more attachment sites for biochar colloid retention. The same non-monotonic retention behavior of biochar colloids as a function of PAHs sorption time was similar to the case in the smooth quartz sand (Fig. 6c and d).

4. Conclusion

Biochar strongly adsorbs organic contaminants and shows a broad potential for the remediation of soils contaminated by organic compounds. After being applied to the field, biochar can be broken down into nano-sized and colloidal particles due to physical, chemical, and biological aging. Nano-sized and colloidal biochar might leach down with irrigation and rainfall from topsoil to subsoil. Because biochar can strongly adsorb organic contaminants, nano-sized and colloidal biochar might facilitate the migration of organic pollutants in the polluted soil and exhibit long-term environmental risk for groundwater. In addition to biochar, other porous adsorbent materials such as activated carbon and fullerene can effectively sequestrate contaminants from the environment. Our study indicated that the fate and mobility of porous colloids and nanoparticles might be affected by kinetic sorption of organic pollutants due to their large internal pores. To estimate the environmental fate of porous colloids and nanoparticles in PAHs-polluted soil or groundwater, it is vital to consider the impact of PAHs sorption kinetics on the fate and transport of porous colloids and nanoparticles.

CRediT authorship contribution statement

Wen Yang: Conceptualization, Methodology, Software, Validation, Formal analysis, Investigation, Resources, Writing – original draft, Writing - review & editing, Visualization. **Ting Qu:** Validation, Investigation. **Markus Flury:** Writing - review & editing. **Xin Zhang:** Validation, Investigation. **Sigmund Gabriel:** Writing - review & editing. **Jianying Shang:** Conceptualization, Methodology, Writing – original draft, Writing - review & editing, Supervision, Project administration, Funding acquisition. **Baoguo Li:** Writing - review & editing, Supervision.

Declaration of Competing Interest

The authors declare that they have no known competing financial interests or personal relationships that could have appeared to influence the work reported in this paper.

Acknowledgments

This work was supported by the National Natural Science Foundation of China (41771255), the USDA-NIFA Hatch Project (1014527), the National Key Research and Development Program (2017YFD0801503), and the “1000-Talents Plan” for Young Researchers.

Appendix A. Supplementary data

Details about the sorption models, PAHs-sorbed biochar preparation, single-collector efficiency, SEM images, and ATR-FTIR spectra of the biochar colloids, and XDLVO interaction between the colloids and sand. Supplementary data to this article can be found online at https://doi.org/10.1016/j.jhydrol.2021.126839.

References

An, X., Xiao, B., Di, X., Dong, H., Tang, H., 2017. Research progress on aging of organic pollutants in geosorbents: a review. Acta Geochimica 36 (1), 27–43. https://doi.org/10.1007/s11631-016-0129-z.

Anyika, C., Abdul Majid, Z., Ibrahim, Z., Zakaria, M.P., Yahya, A., 2015. The impact of biochars on sorption and biodegradation of polycyclic aromatic hydrocarbons in soils–a review. Environ. Sci. Pollut. Res. Int. 22 (5), 3314–3341. https://doi.org/10.1007/s11356-014-3719-5.

Batista, E.M.C.C., Shultz, J., Matos, T.T.S., Fornari, M.R., Ferreira, T.M., Szpoganicz, B., de Freitas, R.A., Mangrich, A.S., 2018. Effect of surface and porosity of biochar on water holding capacity aiming indirectly at preservation of the Amazon biome. Sci. Rep. 8 (1) https://doi.org/10.1038/s41598-018-28794-z.

Beesley, L., Moreno-Jimenez, E., Gomez-Eyles, J.L., 2010. Effects of biochar and greenwaste compost amendments on mobility, bioavailability and toxicity of inorganic and organic contaminants in a multi-element polluted soil. Environ. Pollut. 158 (6), 2282–2287. https://doi.org/10.1016/j.envpol.2010.02.003.

Bradford, S.A., Simunek, J., Bettahar, M., Van Genuchten, M.T., Yates, S.R., 2003. Modeling colloid attachment, straining, and exclusion in saturated porous media. Environ. Sci. Technol. 37 (10), 2242–2250. https://doi.org/10.1021/es025899u.

Břendová, K., Száková, J., Lhotka, M., Krulikovská, T., Punčochář, M., Tlustoš, P., 2017. Biochar physicochemical parameters as a result of feedstock material and pyrolysis temperature: predictable for the fate of biochar in soil? Environ. Geochem. Health 39 (6), 1381–1395. https://doi.org/10.1007/s10653-017-0004-9.

Bu, J., Loh, G., Gwie, C.G., Dewiyanti, S., Tasrif, M., Borgna, A., 2011. Desulfurization of diesel fuels by selective adsorption on activated carbons: Competitive adsorption of polycyclic aromatic sulfur heterocycles and polycyclic aromatic hydrocarbons. Chem. Eng. J. 166 (1), 207–217. https://doi.org/10.1016/j.cej.2010.10.063.

Byrne, C.E., Nagle, D.C., 1997. Carbonization of wood for advanced materials applications. Carbon, 35(2): 259–266. Doi 10.1016/S0008-6223(96)00136-4.

Cao, W., Yin, L., Zhang, D., Wang, Y., Yuan, J., Zhu, Y.i., Dou, J., 2019. Contamination, Sources, and Health Risks Associated with Soil PAHs in Rebuilt Land from a Coking Plant, Beijing, China. Int. J. Environ. Res. Public Health 16 (4), 670. https://doi.org/10.3390/ijerph16040670.

Castan, S., Sigmund, G., Hüffer, T., Hofmann, T., 2019. Biochar particle aggregation in soil pore water: the influence of ionic strength and interactions with pyrene. Environ. Sci-Proc. Imp. 21 (10), 1722–1728. https://doi.org/10.1039/C9EM00277D.

Chan, C.C.V., Lari, K., Soulsbury, K., 2020. An intermittently operated biochar filter to remove chemical contaminants from drinking water. Int. J. Environ. Sci. Technol. 17 (6), 3119–3130. https://doi.org/10.1007/s13762-019-02615-w.

Chen, B., Zhou, D., Zhu, L., 2008. Transitional adsorption and partition of nonpolar and polar aromatic contaminants by biochars of pine needles with different pyrolytic temperatures. Environ. Sci. Technol. 42 (14), 5137–5143. https://doi.org/10.1021/es8002684.

Chen, Z., Chen, B., Chiou, C.T., 2012. Fast and slow rates of naphthalene sorption to biochars produced at different temperatures. Environ. Sci. Technol. 46 (20), 11104–11111. https://doi.org/10.1021/es302345e.

Cornelissen, G., Gustafsson, O., 2005. Importance of unburned coal carbon, black carbon, and amorphous organic carbon to phenanthrene sorption in sediments. Environ. Sci. Technol. 39 (3), 764–769. https://doi.org/10.1021/es049320z.

Cornelissen, G., Breedveld, G.D., Kalaitzidis, S., Christanis, K., Kibsgaard, A., Oen, A.M. P., 2006. Strong Sorption of Native PAHs to Pyrogenic and Unburned Carbonaceous Geosorbents in Sediments. Environ. Sci. Technol. 40 (4), 1197–1203. https://doi.org/10.1021/es052072210.1021/es0520722.s001.

de Jesus, J.H.F., da C. Cunha, G., Cardoso, E.M.C., Mangrich, A.S., Romão, L.P.C., 2017. Evaluation of waste biomasses and their biochars for removal of polycyclic aromatic hydrocarbons. J. Environ. Manage. 200, 186–195. https://doi.org/10.1016/j.jenvman.2017.05.084.

Eeshwarasinghe, D., Loganathan, P., Kalaruban, M., Sounthararajah, D.P., Kandasamy, J., Vigneswaran, S., 2018. Removing polycyclic aromatic hydrocarbons from water using granular activated carbon: kinetic and equilibrium adsorption studies. Environ. Sci. Pollut. Res. 25 (14), 13511–13524. https://doi.org/10.1007/s11356-018-1518-0.

Gao, X.P., Wu, H.W., 2014. Aerodynamic Properties of Biochar Particles: Effect of Grinding and Implications. Environ. Sci. Tech. Let. 1 (1), 60–64. https://doi.org/10.1021/ez400165g.

Gray, M., Johnson, M.G., Dragila, M.I., Kleber, M., 2014. Water uptake in biochars: The roles of porosity and hydrophobicity. Biomass Bioenerg. 61, 196–205. https://doi.org/10.1016/j.biombioe.2013.12.010.

Guo, W., Ai, Y., Men, B., Wang, S., 2017. Adsorption of phenanthrene and pyrene by biochar produced from the excess sludge: experimental studies and theoretical analysis. Int. J. Environ. Sci. Technol. 14 (9), 1889–1896. https://doi.org/10.1007/s13762-017-1272-8.

Hameed, R., Lei, C., Fang, J., Lin, D., 2021. Co-transport of biochar colloids with organic contaminants in soil column. Environ. Sci. Pollut. Res. Int. 28 (2), 1574–1586. https://doi.org/10.1007/s11356-020-10606-5.

Han, X.M., Liu, Y.R., Zheng, Y.M., Zhang, X.X., He, J.Z., 2014. Response of bacterial *pdo1*, *nah*, and $C_{12}O$ genes to aged soil PAH pollution in a coke factory area. Environ. Sci. Pollut. Res. Int. 21 (16), 9754–9763. https://doi.org/10.1007/s11356-014-2928-2.

Wang, H., Fang, C., Wang, Q., Chu, Y., Song, Y., Chen, Y., Xue, X., 2018. Sorption of tetracycline on biochar derived from rice straw and swine manure. RSC Adv. 8 (29), 16260–16268. https://doi.org/10.1039/C8RA01454J.

Jia, H., Zhao, S., Zhu, K., Huang, D., Wu, L., Guo, X., 2018. Activate persulfate for catalytic degradation of adsorbed anthracene on coking residues: Role of persistent free radicals. Chem. Eng. J. 351, 631–640. https://doi.org/10.1016/j.cej.2018.06.147.

Jin, J., Sun, K.e., Wang, Z., Han, L., Du, P., Wang, X., Xing, B., 2017. Effects of chemical oxidation on phenanthrene sorption by grass- and manure-derived biochars. Sci. Total Environ. 598, 789–796. https://doi.org/10.1016/j.scitotenv.2017.04.160.

Kang, S., Jung, J., Choe, J.K., Ok, Y.S., Choi, Y., 2017. Effect of biochar particle size on hydrophobic organic compound sorption kinetics: Applicability of using representative size. Sci. Total Environ. 619–620, 410–418. https://doi.org/10.1016/j.scitotenv.2017.11.129.

Kang, S., Kim, G., Choe, J.K., Choi, Y., 2019. Effect of using powdered biochar and surfactant on desorption and biodegradability of phenanthrene sorbed to biochar. J. Hazard. Mater. 371, 253–260. https://doi.org/10.1016/j.jhazmat.2019.02.104.

Khan, S., Waqas, M., Ding, F., Shamshad, I., Arp, H.P.H., Li, G., 2015. The influence of various biochars on the bioaccessibility and bioaccumulation of PAHs and potentially toxic elements to turnips (Brassica rapa L.). J. Hazard. Mater. 300, 243–253. https://doi.org/10.1016/j.jhazmat.2015.06.050.

Kinney, T.J., Masiello, C.A., Dugan, B., Hockaday, W.C., Dean, M.R., Zygourakis, K., Barnes, R.T., 2012. Hydrologic properties of biochars produced at different temperatures. Biomass Bioenerg. 41, 34–43. https://doi.org/10.1016/j.biombioe.2012.01.033.

Lecoanet, H.F., Wiesner, M.R., 2004. Velocity Effects on Fullerene and Oxide Nanoparticle Deposition in Porous Media. Environ. Sci. Technol. 38 (16), 4377–4382. https://doi.org/10.1021/es035354f.

Leng, L., Xiong, Q., Yang, L., Li, H., Zhou, Y., Zhang, W., Jiang, S., Li, H., Huang, H., 2021. An overview on engineering the surface area and porosity of biochar. Sci. Total Environ. 763, 144204. https://doi.org/10.1016/j.scitotenv.2020.144204.

Li, H., Qu, R., Li, C., Guo, W., Han, X., He, F., Ma, Y., Xing, B., 2014. Selective removal of polycyclic aromatic hydrocarbons (PAHs) from soil washing effluents using biochars produced at different pyrolytic temperatures. Bioresour. Technol. 163, 193–198. https://doi.org/10.1016/j.biortech.2014.04.042.

Li, X.N., Song, Y., Wang, F., Bian, Y.R., Jiang, X., 2019. Combined effects of maize straw biochar and oxalic acid on the dissipation of polycyclic aromatic hydrocarbons and microbial community structures in soil: A mechanistic study. J. Hazard. Mater. 364, 325–331. https://doi.org/10.1016/j.jhazmat.2018.10.041.

Lian, F., Sun, B., Song, Z., Zhu, L., Qi, X., Xing, B., 2014. Physicochemical properties of herb-residue biochar and its sorption to ionizable antibiotic sulfamethoxazole. Chem. Eng. J. 248, 128–134. https://doi.org/10.1016/j.cej.2014.03.021.

Liao, P., Yuan, S., Zhang, W., Tong, M., Wang, K., 2012. Mechanistic aspects of nitrogen-heterocyclic compound adsorption on bamboo charcoal. J. Colloid Interf. Sci. 382 (1), 74–81. https://doi.org/10.1016/j.jcis.2012.05.052.

Liu, C.-H., Chuang, Y.-H., Li, H., Boyd, S.A., Teppen, B.J., Gonzalez, J.M., Johnston, C.T., Lehmann, J., Zhang, W., 2019. Long-term sorption of lincomycin to biochars: The intertwined roles of pore diffusion and dissolved organic carbon. Water Res. 161, 108–118. https://doi.org/10.1016/j.watres.2019.06.006.

Liu, C.-H., Chuang, Y.-H., Li, H., Teppen, B.J., Boyd, S.A., Gonzalez, J.M., Johnston, C.T., Lehmann, J., Zhang, W., 2016. Sorption of Lincomycin by Manure-Derived Biochars from Water. J. Environ. Qual. 45 (2), 519–527. https://doi.org/10.2134/jeq2015.06.0320.

Liu, X., Sun, J.u., Duan, S., Wang, Y., Hayat, T., Alsaedi, A., Wang, C., Li, J., 2017. A valuable biochar from poplar catkins with high adsorption capacity for both organic pollutants and inorganic heavy metal ions. Sci. Rep. 7 (1) https://doi.org/10.1038/s41598-017-09446-0.

Luo, L., Lv, J.T., Chen, Z., Huang, R.X., Zhang, S.Z., 2017. Insights into the attenuated sorption of organic compounds on black carbon aged in soil. Environ. Pollut. 231, 1469–1476. https://doi.org/10.1016/j.envpol.2017.09.010.

Mia, S., Dijkstra, F.A., Singh, B., 2017. Chapter One - Long-term aging of biochar: a molecular understanding with agricultural and environmental implications. Adv. Agron. 141, 1–51. https://doi.org/10.1016/bs.agron.2016.10.001.

Obia, A., Borresen, T., Martinsen, V., Cornelissen, G., Mulder, J., 2017. Vertical and lateral transport of biochar in light-textured tropical soils. Soil Till. Res. 165, 34–40. https://doi.org/10.1016/j.still.2016.07.016.

Oleszczuk, P., Hale, S.E., Lehmann, J., Cornelissen, G., 2012. Activated carbon and biochar amendments decrease pore-water concentrations of polycyclic aromatic hydrocarbons (PAHs) in sewage sludge. Bioresour. Technol. 111, 84–91. https://doi.org/10.1016/j.biortech.2012.02.030.

Peter Atkins, P., De Paula, J., 2014. Atkins' Physical Chemistry. OUP Oxford.

Qiao, K., Tian, W., Bai, J., Dong, J., Zhao, J., Gong, X., Liu, S., 2018. Preparation of biochar from Enteromorpha prolifera and its use for the removal of polycyclic aromatic hydrocarbons (PAHs) from aqueous solution. Ecotox. Environ. Safe. 149, 80–87. https://doi.org/10.1016/j.ecoenv.2017.11.027.

Que, W., Jiang, L., Wang, C., Liu, Y., Zeng, Z., Wang, X., Ning, Q., Liu, S., Zhang, P., Liu, S., 2018. Influence of sodium dodecyl sulfate coating on adsorption of methylene blue by biochar from aqueous solution. J. Environ. Sci. (China) 70, 166–174. https://doi.org/10.1016/j.jes.2017.11.027.

Rein, A., Adam, I.K.U., Miltner, A., Brumme, K., Kästner, M., Trapp, S., 2016. Impact of bacterial activity on turnover of insoluble hydrophobic substrates (phenanthrene and pyrene)—Model simulations for prediction of bioremediation success. J. Hazard. Mater. 306, 105–114. https://doi.org/10.1016/j.jhazmat.2015.12.005.

Shang, J.G., Kong, X.R., He, L.L., Li, W.H., Liao, Q.J.H., 2016. Low-cost biochar derived from herbal residue: characterization and application for ciprofloxacin adsorption. Int. J. Environ. Sci. Technol. 13 (10), 2449–2458. https://doi.org/10.1007/s13762-016-1075-3.

Sharma, P., Flury, M., Mattson, E.D., 2008. Studying colloid transport in porous media using a geocentrifuge. Water Resour. Res. 44 (7), 767–768. https://doi.org/10.1029/2007WR006456.

Sigmund, G., Bucheli, T.D., Hilber, I., Micić, V., Kah, M., Hofmann, T., 2017. Effect of ageing on the properties and polycyclic aromatic hydrocarbon composition of biochar. Environ. Sci-Proc. Imp. 19 (5), 768–774. https://doi.org/10.1039/C7EM00116A.

Sigmund, G., Poyntner, C., Piñar, G., Kah, M., Hofmann, T., 2018. Influence of compost and biochar on microbial communities and the sorption/degradation of PAHs and NSO-substituted PAHs in contaminated soils. J. Hazard. Mater. 345, 107–113. https://doi.org/10.1016/j.jhazmat.2017.11.010.

Šimunek, J., Šejna, M., van Genuchten, M.T., 1998. The HYDRUS-1D software package for simulating the one-dimensional movement of water, heat, and multiple solutes in variably-saturated media, Version 2.0, IGWMC-TPS-70. International Ground Water Modeling Center, Colorado School of Mines, Golden, CO.

Soltani, N., Keshavarzi, B., Moore, F., Tavakol, T., Lahijanzadeh, A.R., Jaafarzadeh, N., Kermani, M., 2015. Ecological and human health hazards of heavy metals and polycyclic aromatic hydrocarbons (PAHs) in road dust of Isfahan metropolis. Iran. Sci. Total Environ. 505, 712–723. https://doi.org/10.1016/j.scitotenv.2014.09.097.

Song, B., Chen, M., Zhao, L., Qiu, H., Cao, X., 2019. Physicochemical property and colloidal stability of micron- and nano-particle biochar derived from a variety of feedstock sources. Sci. Total Environ. 661, 685–695. https://doi.org/10.1016/j.scitotenv.2019.01.193.

Spokas, K.A., Novak, J.M., Masiello, C.A., Johnson, M.G., Colosky, E.C., Ippolito, J.A., Trigo, C., 2014. Physical disintegration of biochar: An overlooked process. Environ. Sci. Tech. Let. 1 (8), 326–332. https://doi.org/10.1021/ez500199t.

Tang, J.C., Lv, H.H., Gong, Y.Y., Huang, Y., 2015. Preparation and characterization of a novel graphene/biochar composite for aqueous phenanthrene and mercury removal. Bioresour. Technol. 196, 355–363. https://doi.org/10.1016/j.biortech.2015.07.047.

Wang, D., Zhang, W., Hao, X., Zhou, D., 2013a. Transport of biochar particles in saturated granular media: effects of pyrolysis temperature and particle size. Environ. Sci. Technol. 47 (2), 821–828. https://doi.org/10.1021/es303794d.

Wang, D., Zhang, W., Zhou, D., 2013b. Antagonistic effects of humic acid and iron oxyhydroxide grain-coating on biochar nanoparticle transport in saturated sand. Environ. Sci. Technol. 47 (10), 5154–5161. https://doi.org/10.1021/es305337r.

Wang, F., Sun, H., Ren, X., Zhang, K., 2017a. Sorption of naphthalene and its hydroxyl substitutes onto biochars in single-solute and bi-solute systems with propranolol as the co-solute. Chem. Eng. J. 326, 281–291. https://doi.org/10.1016/j.cej.2017.05.159.

Wang, H., Chu, Y., Fang, C., Huang, F., Song, Y., Xue, X., Paz-Ferreiro, J., 2017b. Sorption of tetracycline on biochar derived from rice straw under different temperatures. PLoS One 12 (8), e0182776. https://doi.org/10.1371/journal.pone.0182776.

Wang, J., Chen, Z., Chen, B., 2014. Adsorption of polycyclic aromatic hydrocarbons by graphene and graphene oxide nanosheets. Environ. Sci. Technol. 48 (9), 4817–4825. https://doi.org/10.1021/es405227u.

Wang, X., Sato, T., Xing, B., 2006. Competitive sorption of pyrene on wood chars. Environ. Sci. Technol. 40 (10), 3267–3272. https://doi.org/10.1021/es052197710.1021/es0521977.

Wang, Z., Han, L., Sun, K.e., Jin, J., Ro, K.S., Libra, J.A., Liu, X., Xing, B., 2016. Sorption of four hydrophobic organic contaminants by biochars derived from maize straw, wood dust and swine manure at different pyrolytic temperatures. Chemosphere 144, 285–291. https://doi.org/10.1016/j.chemosphere.2015.08.042.

Wu, Q., Liu, Z., Liang, J., Kuo, D.T.F., Chen, S., Hu, X., Deng, M., Zhang, H., Lu, YueHan, 2019. Assessing pollution and risk of polycyclic aromatic hydrocarbons in sewage sludge from wastewater treatment plants in China's top coal-producing region. Environ. Monit. Assess. 191 (2) https://doi.org/10.1007/s10661-019-7225-6.

Xiao, X., Chen, B., Zhu, L., 2014. Transformation, morphology, and dissolution of silicon and carbon in rice straw-derived biochars under different pyrolytic temperatures. Environ. Sci. Technol. 48 (6), 3411–3419. https://doi.org/10.1021/es405676h.

Xiao, X., Liu, D., Yan, Y., Wu, Z., Wu, Z., Cravotto, G., 2015. Preparation of activated carbon from Xinjiang region coal by microwave activation and its application in naphthalene, phenanthrene, and pyrene adsorption. J. Taiwan Inst. Chem. E. 53, 160–167. https://doi.org/10.1016/j.jtice:2015.02.031.

Yakout, S.M., Daifullah, A.A.M., El-Reefy, S.A., 2013. Adsorption of naphthalene, phenanthrene and pyrene from aqueous solution using low-cost activated carbon derived from agricultural wastes. Adsorpt. Sci. Technol. 31 (4), 293–302. https://doi.org/10.1260/0263-6174.31.4.293.

Yang, W., Bradford, S.A., Wang, Y., Sharma, P., Shang, J., Li, B., 2019a. Transport of biochar colloids in saturated porous media in the presence of humic substances or proteins. Environ. Pollut. 246, 855–863. https://doi.org/10.1016/j.envpol.2018.12.075.

Yang, W., Feng, T., Flury, M., Li, B., Shang, J., 2020. Effect of sulfamethazine on surface characteristics of biochar colloids and its implications for transport in porous media. Environ. Pollut. 256, 113482. https://doi.org/10.1016/j.envpol.2019.113482.

Yang, W., Shang, J., Li, B., Flury, M., 2019b. Surface and colloid properties of biochar and implications for transport in porous media. Crit. Rev. Env. Sci. Tec. 50 (23), 2484–2522. https://doi.org/10.1080/10643389.2019.1699381.

Yang, W., Wang, Y., Shang, J., Liu, K., Sharma, P., Liu, J., Li, B., 2017a. Antagonistic effect of humic acid and naphthalene on biochar colloid transport in saturated porous media. Chemosphere 189, 556–564. https://doi.org/10.1016/j.chemosphere.2017.09.060.

Yang, W., Wang, Y., Sharma, P., Li, B., Liu, K., Liu, J., Flury, M., Shang, J., 2017b. Effect of naphthalene on transport and retention of biochar colloids through saturated porous media. Colloid. Surface. A 530, 146–154. https://doi.org/10.1016/j.colsurfa.2017.07.010.

Yang, X.N., Chen, Z.F., Wu, Q.H., Xu, M.Y., 2018. Enhanced phenanthrene degradation in river sediments using a combination of biochar and nitrate. Sci. Total Environ. 619, 600–605. https://doi.org/10.1016/j.scitotenv.2017.11.130.

Yang, Y., Hofmann, T., Pies, C., Grathwohl, P., 2008. Sorption of polycyclic aromatic hydrocarbons (PAHs) to carbonaceous materials in a river floodplain soil. Environ. Pollut. 156 (3), 1357–1363. https://doi.org/10.1016/j.envpol.2008.02.024.

Yargicoglu, E.N., Sadasivam, B.Y., Reddy, K.R., Spokas, K., 2015. Physical and chemical characterization of waste wood derived biochars. Waste Manage. 36, 256–268. https://doi.org/10.1016/j.wasman.2014.10.029.

Ye, S., Zeng, G., Wu, H., Liang, J., Zhang, C., Dai, J., Xiong, W., Song, B., Wu, S., Yu, J., 2019. The effects of activated biochar addition on remediation efficiency of co-composting with contaminated wetland soil. Res. Cons. Recy. 140, 278–285. https://doi.org/10.1016/j.resconrec.2018.10.004.

Yin, K., Viana, P.Z., Rockne, K.J., 2019. Organic contaminated sediments remediation with active caps: Nonlinear adsorption unveiled by combined isotherm and column transportation studies. Chemosphere 214, 710–718. https://doi.org/10.1016/j.chemosphere.2018.09.122.

Zeng, Z.-W., Tan, X.-F., Liu, Y.-G., Tian, S.-R., Zeng, G.-M., Jiang, L.-H., Liu, S.-b., Li, J., Liu, N.i., Yin, Z.-H., 2018. Comprehensive adsorption studies of doxycycline and ciprofloxacin antibiotics by biochars prepared at different temperatures. Front. Chem. 6 https://doi.org/10.3389/fchem.2018.00080.

Zhang, M., Shu, L., Guo, X., Shen, X., Zhang, H., Shen, G., Wang, B., Yang, Y.u., Tao, S., Wang, X., 2015. Impact of humic acid coating on sorption of naphthalene by biochars. Carbon 94, 946–954. https://doi.org/10.1016/j.carbon.2015.07.079.

Zhang, P., Zheng, S., Liu, J., Wang, B., Liu, F., Feng, Y., 2018. Surface properties of activated sludge-derived biochar determine the facilitating effects on Geobacter co-cultures. Water Res. 142, 441–451. https://doi.org/10.1016/j.watres.2018.05.058.

Zhang, W., et al., 2010. Transport and retention of biochar particles in porous media: effect of pH, ionic strength, and particle size. Ecohydrology 3 (4), 497–508. https://doi.org/10.1002/eco.160.

Zhu, D., Pignatello, J.J., 2005. Characterization of Aromatic Compound Sorptive Interactions with Black Carbon (Charcoal) Assisted by Graphite as a Model. Environ. Sci. Technol. 39 (7), 2033–2041. https://doi.org/10.1021/es049137610.1021/es0491376.s001.

Zhu, X., Wang, Y., Zhang, Y., Chen, B., 2018. Reduced bioavailability and plant uptake of polycyclic aromatic hydrocarbons from soil slurry amended with biochars pyrolyzed under various temperatures. Environ. Sci. Pollut. Res. Int. 25 (17), 16991–17001. https://doi.org/10.1007/s11356-018-1874-9.